Yrast level structure of the neutron deficient $N=49$ isotones ^{92}Tc, ^{93}Ru, ^{94}Rh, and ^{95}Pd up to high angular momentum

S. E. Arnell, D. Foltescu, H. A. Roth, and Ö. Skeppstedt
Department of Physics, Chalmers University of Technology and The University of Gothenburg, S-412 96 Göteborg, Sweden

J. Blomqvist and A. Nilsson
The Manne Siegbahn Institute, S-104 05 Stockholm, Sweden

T. Kuroyanagi and S. Mitarai
Department of Physics, Kyushu University, Hakozaki, Fukuoka, 812 Japan

J. Nyberg*
Niels Bohr Institute, DK-4000 Roskilde, Denmark
(Received 9 June 1993)

The projectile-target system ^{40}Ca+^{58}Ni has been used to produce the neutron deficient $N=49$ isotones ^{92}Tc, ^{93}Ru, ^{94}Rh, and ^{95}Pd. The multidetector array NORDBALL including particle selection was used. The yrast level scheme could in three cases be determined up to and above spin values corresponding to the highest angular momenta attainable in the previously used configuration spaces for shell model calculations. The yrast level schemes of the $N=49$ isotones bear a striking relationship to those of the corresponding $N=50$ isotones. By interpreting the experimental high spin yrast structure in shell model configurations we hope to facilitate the choice of a restricted configuration space to be used for calculations. Generally, there is an intrinsic simplicity in most of the observed yrast or near-yrast states.

PACS number(s): 23.20.Lv, 25.70.Jj, 21.60.Cs, 27.60.+j

I. INTRODUCTION

Shell-model calculations for $N=49$ isotones have been performed by Serduke, Lawson, and Gloeckner [1], and Gross and Frenkel [2], all using a $^{88}_{38}$Sr core. Recently Sinatkas *et al.* [3] examined the structure of the $Z,N \leq 50$ nuclei in a model space consisting of the $g_{9/2}$, $p_{1/2}$, $p_{3/2}$, and $f_{5/2}$ hole orbitals inside the doubly closed $^{100}_{50}$Sn core. Generally the models fairly well reproduce the low-lying yrast levels.

In the present work the $N=49$ nuclei $^{92}_{43}$Tc, $^{93}_{44}$Ru, $^{94}_{45}$Rh, and $^{95}_{46}$Pd have been studied. Yrast states of high angular momentum of both parities appear at low excitation energy due to the coupling of the valence protons and the neutron hole in $1g_{9/2}$ and $2p_{1/2}$ orbitals. The use of multidetector arrays, in the present case NORDBALL with particle selection [4], allows the yrast level scheme to be determined up to spin values corresponding to the highest angular momenta attainable in the configuration space used for the calculations. Thus experimental and theoretical yrast levels can now be compared over a large range of excitation energies.

The maximum angular momenta that can be generated in a model space limited to $f_{5/2}$, $p_{3/2}$, $p_{1/2}$, and $g_{9/2}$ orbitals can be calculated for the $N=49$ isotones mentioned above. They are given in Table I together with the pertinent configurations, and are generated from expressions of the type $\pi(f_{5/2})^{-1}\pi(p_{1/2})^{1}\pi(g_{9/2})^{5-8}\nu(g_{9/2})^{-1}$ for positive-parity states and $\pi(f_{5/2})^{-1}\pi(p_{1/2})^{2}\pi(g_{9/2})^{4-7}\nu(g_{9/2})^{-1}$ for negative-parity states. The experimental maximum values can be compared to those given in Table I and it can be decided if the configuration space chosen is appropriate for the description of the states observed. If not, larger configuration spaces must be chosen, i.e., we have to break the $N=50$ neutron shell closure by promoting one $g_{9/2}$ neutron to the subshells above. By interpreting the experimental high-spin yrast structure in terms of shell-model configurations we hope to facilitate the choice of a restricted configuration space to be used for calculations.

Up to the present work the following experimental information was known about the $N=49$ isotones mentioned above: High-spin states in ^{92}Tc have been studied by Fields *et al.* [5]. Levels up to 12^+ were identified. The level structure of ^{93}Ru has previously been studied by Nilsson and Grecescu [6] using the ^{92}Mo$(\alpha,3n)^{93}$Ru reaction. Levels with spin values $\frac{13}{2}^+$ and $\frac{17}{2}^+$ were suggested. Three isomeric states are known [7]. Two states with spin values (3^+) and (8^+), respectively, are known in ^{94}Rh [8]. The relative positions of these isomeric states are unknown. The (8^+) state could be the ground state. Some γ rays following the decay of ^{94}Pd are known [9] but no level scheme for ^{94}Rh is established.

Nolte and Hick [10] investigated the residual activities of the projectile-target system ^{40}Ca+^{58}Ni. A β-decaying

*Present address: The Svedberg Laboratory, Uppsala University, S-751 21 Uppsala, Sweden.

TABLE I. $N=49$ isotones with pertinent configurations.

Nucleus $N=49$	$(p_{1/2},g_{9/2})$	Theory, configuration space: $(f_{5/2},p_{3/2},p_{1/2},g_{9/2})$ Maximum spin values	$(p_{1/2},g_{9/2},d_{5/2})$
$^{92}_{43}$Tc	17^+	20^+	23^+
	17^-	19^-	23^-
$^{93}_{44}$Ru	$33/2^+$	$39/2^+$	$45/2^+$
	$35/2^-$	$39/2^-$	$47/2^-$
$^{94}_{45}$Rh	17^+	18^+	23^+
	17^-	19^-	23^-
$^{95}_{46}$Pd	$33/2^+$	$33/2^+$	$45/2^+$
	$31/2^-$	$35/2^-$	$43/2^-$

high-spin isomer in ^{95}Pd with $J^\pi=(\frac{21}{2}^+)$, a half-life of 14 s, and an excitation energy of about 2 MeV was proposed.

II. EXPERIMENTAL PROCEDURES

The nuclei ^{92}Tc, ^{93}Ru, ^{94}Rh, and ^{95}Pd were produced in ^{40}Ca+^{58}Ni collisions at $E(^{40}\text{Ca})=180$ MeV using a stacked target consisting of three self-supporting foils with a thickness of 0.33 mg/cm^2 each (^{58}Ni enrichment 99.7%). The thin foils were at 0.21 mm distance from each other, and were followed by a beam catcher 20 mm downstream. Doppler shift corrections were based on the best fit value $\beta=v/c=3.7\%$. About 55×10^6 events were recorded of which, according to a CASCADE calculation [11], 22 mb of the total cross section of 760 mb ($l_{\max}\approx56\hbar$) constituted the $5pn$ reaction channel leading to ^{92}Tc, 105 mb the $4pn$ channel leading to ^{93}Ru, 14 mb the $3pn$ channel leading to ^{94}Rh, and <1 mb the $2pn$ channel leading to ^{95}Pd. In another experiment the same nuclei were produced at $E(^{40}\text{Ca})=187$ MeV using a 10 mg/cm^2 ^{58}Ni target. About 60×10^6 events were recorded. A short run at $E(^{40}\text{Ca})=147$ MeV, corresponding to the maximum cross sections for ^{94}Rh and ^{95}Pd, facilitated the analysis of these nuclei (cross sections 40 and 8 mb, respectively).

Thick targets have the advantage of producing sharp γ lines as the stopping time of the recoiling ions are of the order of a few ps, while for stacked targets Doppler shift corrections must be introduced and broader γ lines are produced.

The advantages of stacked targets are the following: (i) Isomeric states in the region 0.1–10 ns can be identified and their lifetimes determined. (ii) When adding spectra from the rings of detectors at different angles without applying Doppler compensation (producing $\beta=0$ spectra), sharp lines appear in the decay of isomeric states of appropriate lifetimes which allows coincidence spectroscopy on the succeeding γ decay. (iii) By varying the β value of the Doppler shift correction, target contaminations can easily be traced. For a given contaminant, sharp lines appear for the correct β value. An example is the reactions following ^{40}Ca+^{12}C collisions in our case.

The particle beams, having intensities of the order of 1 particle nA, were delivered by the tandem booster accelerator at NBI, Risø, Denmark. The γ rays were detected in 15 HPGe detectors situated in three rings of the NORDBALL frame [12] at 79°, 101°, and 143° relative to the beam direction. The detectors were energy and efficiency calibrated with ^{56}Co, ^{152}Eu, and ^{133}Ba sources.

The present investigation was performed at a high projectile energy in order to enhance high-spin states and to get large yields from a number of residual nuclei of interest for the present investigation. This means that we had to use a very efficient particle selection system in order to select among the large number of outgoing particle combinations (21 exit channels with cross sections ≥1 mb). Such a system [4] was developed for the NORDBALL detection system in a collaboration between Kyushu University, Japan [13] and Chalmers University of Technology, Sweden [14]. In the present setup the system was adapted for spectroscopy of nuclei far from stability by having 11 liquid scintillator detectors forming a "neutron wall" [14] in the forward hemisphere and detecting evaporated protons and α particles by a 4π Si ball consisting of 21 detectors [13]. The master gate (open for about 100 ns) consisted of a $\gamma\gamma$ event in the Ge detectors in combination with the detection of at least one charged particle in the Si ball.

III. SELECTION OF REACTION CHANNELS

The system used for NORDBALL [4] (Fig. 1) selects among a large number of outgoing particle combinations. Some design criteria and the use of the system will be described below.

The following facts were considered in the design of the system: (i) All particle angular distributions are peaked and have high energy in the forward direction. (ii) The individual detector elements for charged particles can be made to have almost 100% intrinsic efficiency which is not practically possible for the neutron detector elements. (iii) Neutron detectors may replace Ge detectors in a number of the twenty hexagon positions in addition to the free pentagon positions of the NORDBALL frame in order to increase the total detection efficiency for neutrons. (iv) The $\gamma\gamma$-coincidence efficiency is proportional to $N(N-1)$, N being the number of Ge detectors ($N_{\max}=20$). As regards the detection of the charged particles, it can be noted that in spite of the almost 100% detection efficiency of the 21 individual detector elements making up the Si ball, the total efficiency values are

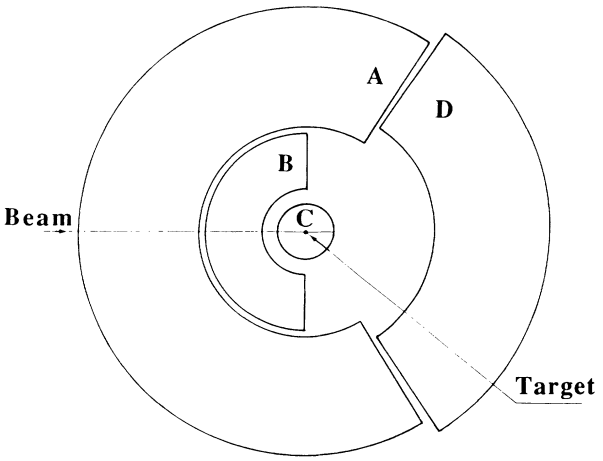

FIG. 1. Schematic picture illustrating the actual configuration of the NORDBALL detector system: (A) Ge array (15 HPGe detectors), (B) 2π BaF_2 ball (30 BaF_2 crystals), (C) 4π Si ball (21 detectors), and (D) neutron wall (11 liquid scintillator detectors, of which 5 are situated in the hexagon positions in the NORDBALL frame).

$\varepsilon_p = 0.80$ and $\varepsilon_\alpha = 0.65$ as quoted by Kuroyanagi *et al.* [13]. These values, which are in fact quite high, reflect that the beam must enter and leave the ball, the target and its support give absorption, etc. However, the appearance of these numbers in powers in the efficiency values for high multiplicity events implies the following: (i) A substantial reduction in statistics for the channel giving the residual nucleus in question, especially for channels with high particle multiplicity. (ii) A "contamination" by the lost events of the matrices of all lower multiplicity channels.

The statements made above have some consequences for the neutron detection: A high neutron detection efficiency, i.e., many neutron detectors, implies a very much reduced $\gamma\gamma$-coincidence efficiency. With 16, 11, or 6 neutron detectors, of which six are placed in the pentagon positions, the relative numbers for the $\gamma\gamma$-coincidence efficiency are 9, 21, and 38, respectively. As a compromise 11 neutron detectors were used in our work.

The kinematical forward focusing facilitates the neutron detection but this is somewhat counteracted by the increased neutron energies. About 50% intrinsic detection efficiency can be expected at the highest neutron energies (about 10 MeV) in the forward direction [14]. For the present setup the total neutron efficiency is $\varepsilon_n \approx 0.25$.

In short, the low detection efficiency for neutrons and the difficulty of obtaining ε values for charged particles very close to 100% are the main deficiencies of our system for selection of reaction channels. All other defects, like scattering of neutrons between the detectors, the possibility of misinterpreting $2p$ events as α-particle events, etc., are of minor importance in comparison. Anyhow, arrangements of this type work in a very impressive way as regards channel selection, being presently the most efficient ones available as regards high-spin spectroscopy for cases with many outgoing reaction channels. Accordingly, NORDBALL with particle selection [4] is an excellent tool for systematic investigations of nuclear structure of a broad mass region in a single experiment.

IV. DATA REDUCTION AND EXPERIMENTAL RESULTS

The general procedure of finding a clean $\gamma\gamma$-coincidence matrix for a certain residual nucleus starts by setting a gate in the particle identification spectrum for the channel in question—with the neutron conditions included, if appropriate. The "raw" matrix so obtained is corrected for "feedthrough" from matrices of higher particle multiplicity. This requires a good knowledge of the projected spectra from all channels of higher multiplicity. The subtraction procedure is performed by a trial and error method.

In the present case the "raw" $\gamma\gamma$-coincidence matrices, obtained by sorting all events associated with $5pn$ to $2pn$ emissions, were corrected for contributions from reaction channels of higher proton multiplicities as well as from other contributing channels.

In the construction of the level schemes, the γ rays were placed in the scheme by use of $\gamma\gamma$-coincidence relations and γ-ray intensities. The computer program ESCL8R [15] was used for control of the level schemes. This program allows fast and easy inspection and fitting of the $\gamma\gamma$ matrix and is used to construct coincidence spectra based on assumed decay patterns, which are then compared to the observed spectra. In this way the program works backwards from the proposed level scheme, and attempts to reproduce the observed $\gamma\gamma$ matrix.

Information on the γ-ray anisotropies was extracted from projected spectra recorded at 79°, 101°, and 143° with respect to the beam axis. The assignment of level spins was mostly based on these anisotropies, defined as $R = 2I(143°)/[I(79°)+I(101°)]$. Considering the high angular momentum brought into the compound system, we assume that essentially all observed transitions have $J_i \geq J_f$ and most transitions have $J_i > J_f$. Crossover transitions are generally expected to be of $E2$ character.

A. Results for ^{92}Tc

In their study of high-spin states in ^{92}Tc, Fields *et al.* [5] proposed a cascade, 2549 keV, $(12^+) \rightarrow$2003 keV, $(11^+) \rightarrow$1355 keV, $10^+ \rightarrow$686 keV, $9^+ \rightarrow 8^+$ (g.s.). Our ^{92}Tc decay scheme, established from $\gamma\gamma$-coincidence relations, is shown in Fig. 2. The scheme consists of two decay sequences with the joint γ flux channeled through the cascade from the 1355 keV, 10^+ state to the ground state. Our spectrum with a gate on the 1355 keV line is shown in Fig. 3.

In a search for isomeric states, the spectrum of $\gamma\gamma$ coincidences from the thin stacked target run showed sharp lines in the spectra that were uncorrected for Doppler shift. The lines and the coincidence relations obtained were those corresponding to the decay of the 2001 keV state. Figure 4 displays a projected spectrum, corrected for Doppler shift, of the 143° ring showing the 1355 keV line. The line is split, showing a very sharp (i.e., not Doppler broadened) peak adjacent to the 1355

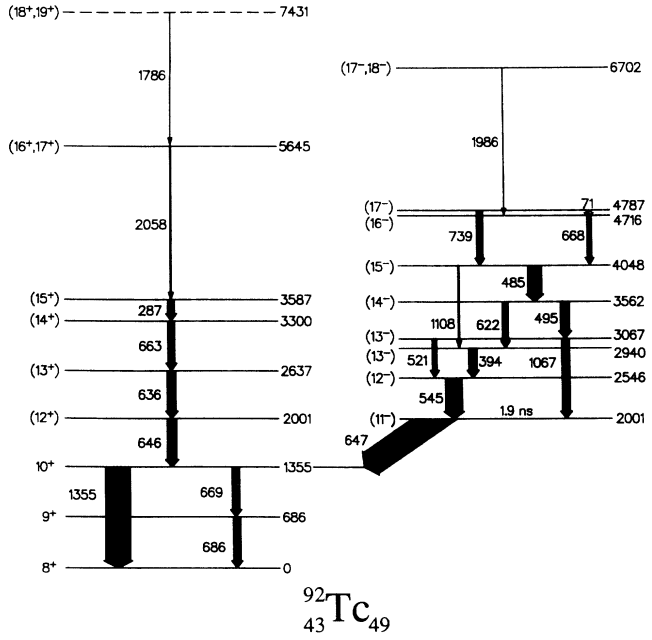

FIG. 2. Tentative level scheme for ^{92}Tc as populated in the ^{58}Ni(^{40}Ca,5*pn*)^{92}Tc reaction. The γ-ray intensities are roughly proportional to the widths of the arrows. Energies are in keV.

keV peak. From the intensity ratio between these peaks and tabulated values of stopping power [16], the lifetime of the isomeric state was determined to 1.9±0.4 ns (after correction for the prompt positive-parity part, as well as for deorientation).

Using the 1355 keV $10^+ \rightarrow 8^+$ (g.s.) transition as an indicator, coincidence spectra gated on the sequence 287, 663, and 636 keV showed only a line of normal width in the Doppler-shift-corrected spectrum, i.e., no lifetime in the ns range is present. Coincidence spectra gated on the 394, 485, 495, 545, 622, and 1067 keV lines, however, gave a Doppler-split 1355 keV line. We see two possible explanations for this behavior. There may be two close-lying levels at 2001 keV deexciting by 646 and 647 keV lines or, alternatively, there may be an isomeric level above and rather close to the 2001 keV level. The low-energy transition connecting the two levels and deexciting the isomeric level may be highly converted and difficult to observe in our setup.

We favor the first alternative because the 646 keV transition in the prompt cascade would then deexcite a state with the spin assignment 11^+ or 12^+. A 647 keV transition from a 1.9 ns isomeric state would have a transition strength of $B(E1)=0.5\times10^{-6}$ W.u., or $B(E2)\approx0.1$ W.u. An $M1$ transition would be retarded by a factor of 2×10^4, and thus be unreasonably slow. Nuclei in this mass region have transition strengths of the order of a few $\times10^{-6}$ W.u. for $E1$ and a few W.u. for $E2$ transitions. As it would be exceptional if a negative-parity sequence would be completely missing we suggest a $J^\pi=11^-$ state close to the 11^+ or 12^+ state.

Fields *et al.* [5] measured angular distributions and

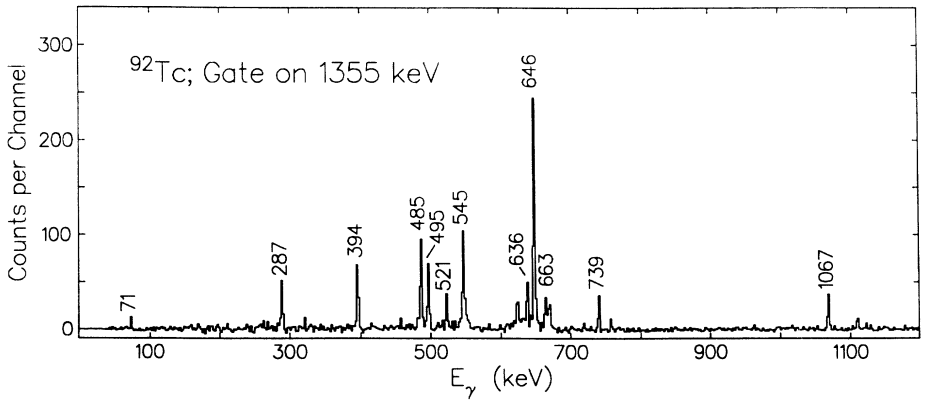

FIG. 3. $\gamma\gamma$-coincidence spectrum (from thick target run) of ^{92}Tc with a gate on the 1355 keV transition. Note the intensity of the 646 keV line.

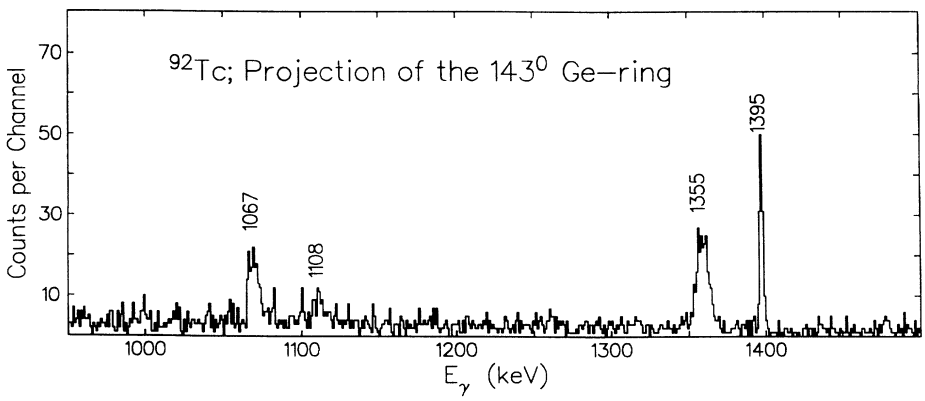

FIG. 4. Part of the 5*pn* matrix projection from the 143° Ge ring (stacked target run, $\beta=3.7\%$). The spectrum shows the unshifted and the shifted components of the 1355 keV line, deexciting the 10^+ level in ^{92}Tc.

TABLE II. Gamma-ray energies, intensities, and anisotropy ratios for γ-ray transitions assigned to ^{92}Tc.

E_γ[a] (keV)	I_γ[b]	R[c]	Tentative assignment $J_i^\pi \rightarrow J_f^\pi$
70.6	11(2)	0.81(9)	$17^- \rightarrow 16^-$
286.9	20(3)	0.93(19)	$15^+ \rightarrow 14^+$
393.6	30(3)	0.66(12)	$13_1^- \rightarrow 12^-$
484.6	55(6)	0.77(11)	$15^- \rightarrow 14^-$
494.7(doublet)	42(5)	0.67(11)	$14^- \rightarrow 13_2^-$
521.0	23(4)	0.93(25)	$13_2^- \rightarrow 12^-$
545.0	69(7)	0.78(11)	$12^- \rightarrow 11^-$
622.2	22(4)	0.71(25)	$14^- \rightarrow 13_1^-$
636.3	29(4)	0.95(18)	$13^+ \rightarrow 12^+$
646.3[d]	$127(12)-x$		$12^+ \rightarrow 10^+$
		1.25(12)	
646.8[d]	x		$11^- \rightarrow 10^+$
662.9	26(3)	0.86(17)	$14^+ \rightarrow 13^+$
668.5[d]	$57(6)-x$		$16^- \rightarrow 15^-$
		0.84(12)	
668.7[d]	x		$10^+ \rightarrow 9^+$
685.6	35(4)	0.66(22)	$9^+ \rightarrow 8^+$
738.6	27(4)	1.55(41)	$17^- \rightarrow 15^-$
1066.7	27(4)	1.47(44)	$13_2^- \rightarrow 11^-$
1108.0	12(3)	1.25(65)	$15^- \rightarrow 13_1^-$
1355.0	100(7)	1.42(19)	$10^+ \rightarrow 8^+$
1785.6	4(1)	1.36(72)	$18^+, 19^+ \rightarrow 16^+, 17^+$
1985.6	7(2)	1.84(87)	$17^-, 18^- \rightarrow 16^-$
2058.3	8(2)		$16^+, 17^+ \rightarrow 15^+$

[a] $\Delta E_\gamma = \pm(0.2-1.0)$ keV depending on the energy and intensity of the transition.
[b] The γ-ray intensity, I_γ, is corrected for detection efficiency and is normalized to 100 for the 1355.0 keV transition.
[c] The γ-ray anisotropy is defined as $R = 2I(143°)/[I(79°)+I(101°)]$.
[d] Not resolved.

quote a_2 and a_4 coefficients of typical stretched $M1$ type for the 686 and 669 keV lines. The 1355 keV line had a probable $E2$ distribution. The a_2 coefficient given for the 647 keV line (-0.08 ± 0.04) is, however, not in accordance with our R value, which hints at a doublet nature of this γ line, combined with different population of the emitting levels in the two reactions.

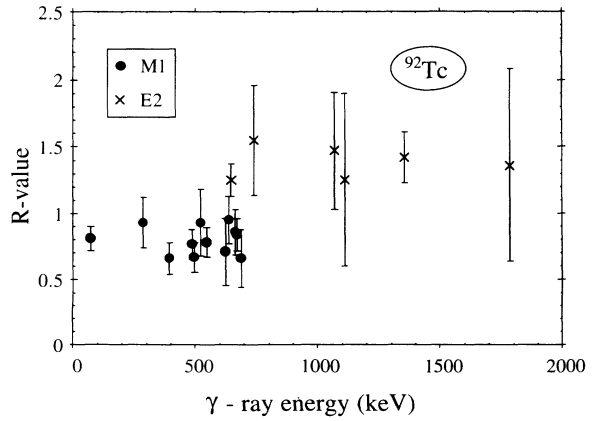

FIG. 5. γ-ray anisotropies, R (see text), plotted vs the energies of the γ-ray transitions in ^{92}Tc.

It can be noted that an alternative position for the 1786 keV line is a direct transition to the (15^+) state at 3587 keV giving a level at 5372 keV.

Table II gives the γ-ray energies, relative intensities, intensity anisotropies, and the position of the transitions in the proposed level scheme of ^{92}Tc. A plot of the R values is given in Fig. 5.

B. Results for ^{93}Ru

According to Nuclear Data Sheets (NDS) [7] the available information about the level structure of ^{93}Ru consists of five states with spin values $\frac{17}{2}^-$(35 ns), $\frac{15}{2}^+$, $\frac{21}{2}^+$(2.15 μs), $\frac{17}{2}^+$, and $\frac{13}{2}^+$, the last state decaying directly to the $\frac{9}{2}^+$ ground state. A spectrum from the stacked target run uncorrected for Doppler shift showed sharp lines at 168, 177, 544, and 1392 keV, i.e., the cascade deexciting the 35 ns isomer. A spectrum gated by the 168 keV transition is shown in Fig. 6. This spectrum shows also a line at 721 keV, i.e., a transition between the $\frac{15}{2}^+$ and the $\frac{13}{2}^+$ states, thus establishing the $\frac{15}{2}^+$ state at 2113 keV (reversing the order of the 168 and 177 keV lines compared to the scheme given in NDS [7]). The level scheme of ^{93}Ru is shown in Fig. 7. Further details re-

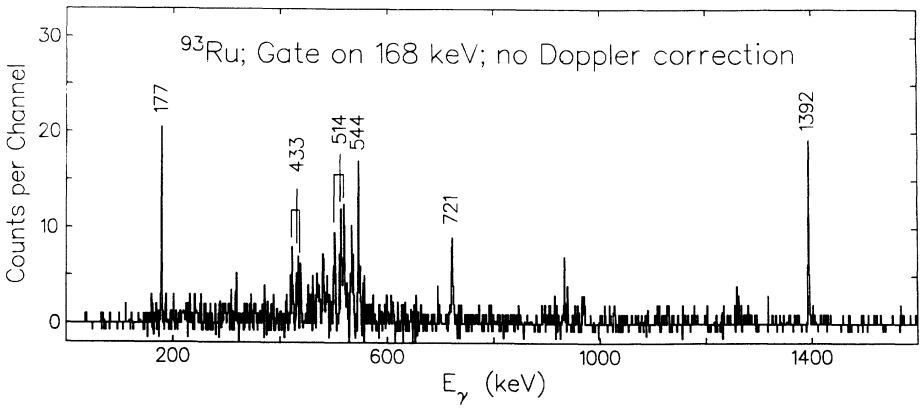

FIG. 6. Spectrum of γ-ray transitions in ^{93}Ru (from stacked target run) uncorrected for Doppler shift; the spectrum is gated by the 168 keV transition and shows the decay of the 35 ns isomeric state.

garding the region 1392–2280 keV are reproduced in Fig. 8 in order to avoid clutter.

A characteristic feature of the yrast level scheme of ^{93}Ru is the existence of energy gaps of the order of more than 2 MeV both in the positive- and negative-parity sequence of levels. Above the gaps a structure of relatively high level density extends to spin values of the order of $\frac{47}{2}$. The main part of the γ flux is channeled through the 514-602-387-651 keV cascade and is interrupted by the long-lived 2.15 μs, 2083 keV, $\frac{21}{2}^+$ state.

Figures 10 and 11 show a few $\gamma\gamma$-coincidence spectra. Table III gives γ-ray energies, relative intensities, anisotropies, and the placement of the transitions in the proposed level scheme of ^{93}Ru. The R values are plotted in Fig. 9.

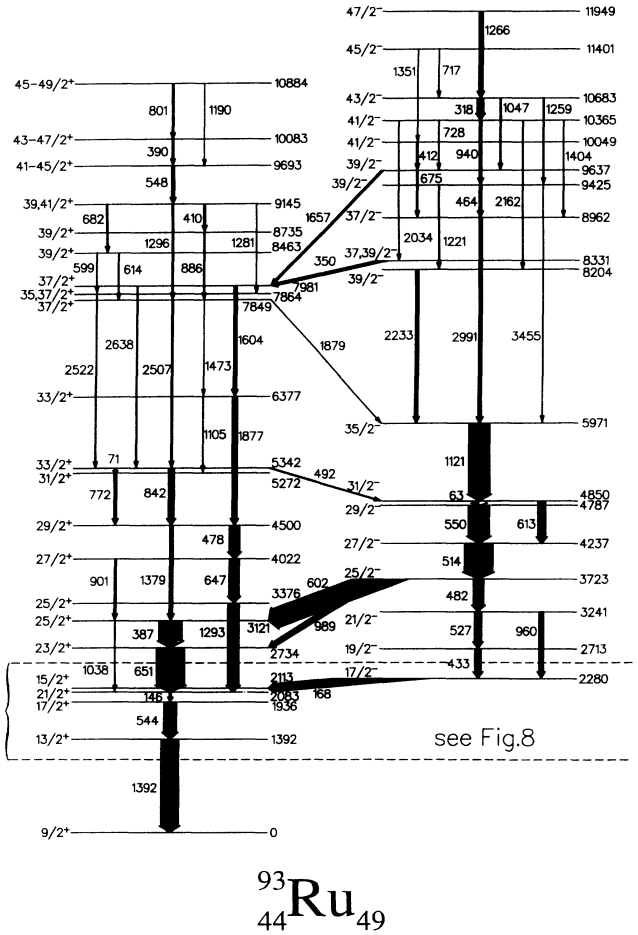

FIG. 7. Tentative level scheme for ^{93}Ru as produced in the ^{58}Ni(^{40}Ca,4pn)^{93}Ru reaction. Energies are in keV. In order to avoid clutter the part of the low-energy structure, marked in the figure, is produced in Fig. 8.

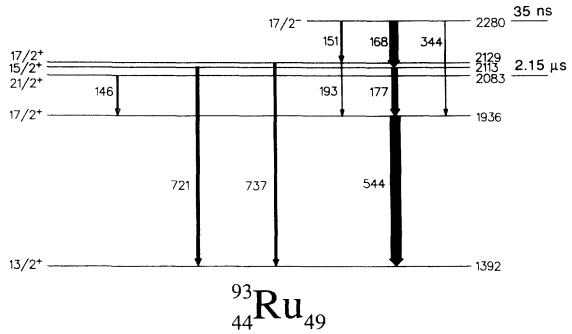

FIG. 8. Part of the level scheme showing details at low excitation energy (up to the 2280 keV, $\frac{17}{2}^-$ level) for ^{93}Ru as produced in the ^{58}Ni(^{40}Ca,4pn)^{93}Ru reaction. Energies are in keV.

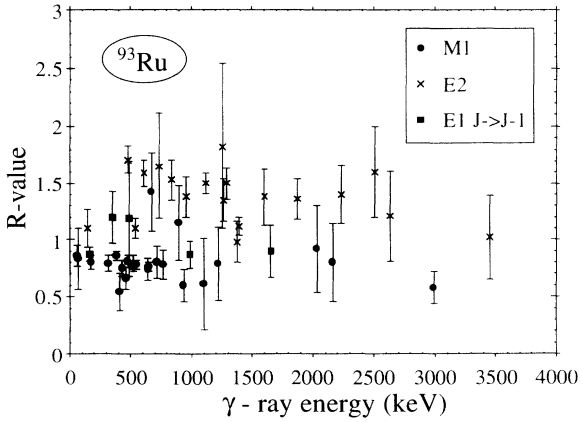

FIG. 9. γ-ray anisotropies, R (see text), plotted vs the energies of the γ-ray transitions in ^{93}Ru.

TABLE III. Gamma-ray energies, intensities, and anisotropy ratios for γ-ray transitions assigned to ^{93}Ru.

E_γ[a] (keV)	I_γ[b]	R[c]	Tentative assignment $J_i^\pi \rightarrow J_f^\pi$
63.1	218(21)	0.86(9)	$31/2^- \rightarrow 29/2^-$
71.2	44(7)	0.83(27)	$33/2_1^+ \rightarrow 31/2^+$
146.3	54(5)	1.10(17)	$21/2^+ \rightarrow 17/2_1^+$
151.3	72(5)	1.09(15)	$17/2^- \rightarrow 17/2_2^+$
167.8	305(12)	0.87(6)	$17/2^- \rightarrow 15/2^+$
176.6	194(8)	0.80(6)	$15/2^+ \rightarrow 17/2_1^+$
193.3	46(9)		$17/2_2^+ \rightarrow 17/2_1^+$
318.3	230(12)	0.79(7)	$43/2^- \rightarrow 41/2_2^-$
343.8	31(8)		$17/2^- \rightarrow 17/2_1^+$
349.9	100(11)	1.20(23)	$(37,39)/2^- \rightarrow 37/2_3^+$
387.2	821(24)	0.86(4)	$25/2_1^+ \rightarrow 23/2^+$
389.7	57(13)	0.45(19)	$(43-47)/2^+ \rightarrow (41-45)/2^+$
410.0	71(9)	0.91(32)	$(39,41)/2^+ \rightarrow 39/2_2^+$
411.8	59(9)	0.54(16)	$41/2_1^- \rightarrow 39/2_3^-$
432.6	241(13)	0.75(7)	$19/2^- \rightarrow 17/2^-$
463.6	101(8)	0.66(10)	$39/2_2^- \rightarrow 37/2^-$
478.1	381(16)	0.81(5)	$29/2^+ \rightarrow 27/2^+$
482.1	376(16)	1.71(12)	$25/2^- \rightarrow 21/2^-$
492.4	36(9)	1.19(51)	$33/2_1^+ \rightarrow 31/2^-$
514.3	1076(33)	0.77(3)	$27/2^- \rightarrow 25/2^-$
527.1	257(14)	0.79(7)	$21/2^- \rightarrow 19/2^-$
544.3	459(21)	1.10(9)	$17/2_1^+ \rightarrow 13/2^+$
548.1	104(28)		$(41-45)/2^+ \rightarrow (39-41)/2^+$
550.3	754(28)	0.78(4)	$29/2^- \rightarrow 27/2^-$
598.8			$39/2_1^+ \rightarrow (35-37)/2^+$
601.5	717(24)	1.68(8)	$25/2^- \rightarrow 25/2_1^+$
613.0	286(15)	1.59(12)	$31/2^- \rightarrow 27/2^-$
614.4	30(10)		$39/2_1^+ \rightarrow 37/2_1^+$
646.6	359(25)	0.74(10)	$27/2^+ \rightarrow 25/2_2^+$
651.2	1000(23)	0.76(4)	$23/2^+ \rightarrow 21/2^+$
675.0	53(7)	1.42(35)	$39/2_3^- \rightarrow 37/2^-$
682.0	52(7)	0.94(24)	$(39,41)/2^+ \rightarrow 39/2_1^+$
716.8	19(8)		$45/2^- \rightarrow 43/2^-$
720.7	117(12)	0.80(14)	$15/2^+ \rightarrow 13/2^+$
728.4	19(7)		$41/2_2^- \rightarrow 39/2_3^-$
737.3	85(14)	1.65(46)	$17/2_2^+ \rightarrow 13/2^+$
771.5	108(11)	0.78(13)	$31/2^+ \rightarrow 29/2^+$
800.7	61(9)	0.45(15)	$(45-49)/2^+ \rightarrow (43-47)/2^+$
842.3	220(13)	1.53(18)	$33/2_1^+ \rightarrow 29/2^+$
886.0	44(7)		$39/2_2^+ \rightarrow 37/2_1^+$
900.7	71(11)	1.15(33)	$27/2^+ \rightarrow 25/2_1^+$
939.6	100(13)	0.60(14)	$41/2_2^- \rightarrow 39/2_2^-$
960.1	174(13)	1.38(18)	$21/2^- \rightarrow 17/2^-$
989.1	181(14)	0.87(12)	$25/2^- \rightarrow 23/2^+$
1038.4	21(7)		$25/2_1^+ \rightarrow 21/2^+$
1046.5	46(8)		$43/2^- \rightarrow 39/2_3^-$
1104.8	26(10)	0.61(40)	$33/2_2^+ \rightarrow 31/2^+$
1120.9	758(29)	1.50(9)	$35/2^- \rightarrow 31/2^-$
1190.5			$(45-49)/2^+ \rightarrow (41-45)/2^+$
1221.3	36(8)	0.79(32)	$39/2_2^- \rightarrow 39/2_1^+$
1266.1	157(13)	1.35(19)	$47/2^- \rightarrow 43/2^-$
1258.7	35(8)	1.82(72)	$43/2^- \rightarrow 39/2_2^-$
1280.8			$(39,41)/2^+ \rightarrow (35,37)/2^+$
1293.1	419(23)	1.50(14)	$25/2_2^+ \rightarrow 21/2^+$
1296.4	64(13)	1.37(61)	$(39,41)/2^+ \rightarrow 37/2_1^+$
1351.4			$45/2^- \rightarrow 41/2_1^-$
1379.2	134(13)	0.98(18)	$29/2^+ \rightarrow 25/2_1^+$

TABLE III (*Continued.*)

E_γ[a] (keV)	I_γ[b]	R[c]	Tentative assignment $J_i^\pi \rightarrow J_f^\pi$
1392.0	637(27)	1.12(8)	$13/2^+ \rightarrow 9/2^+$
1403.9	19(7)	0.57(33)	$41/2_2^- \rightarrow 37/2^-$
1473.1	12(5)		$37/2_1^+ \rightarrow 33/2_2^+$
1604.0	130(13)	1.38(25)	$37/2_3^+ \rightarrow 33/2_2^+$
1656.5	71(11)	0.90(23)	$39/2_3^- \rightarrow 37/2_3^+$
1876.9[d]	$191(16)-x$	1.36(18)	$33/2_2^+ \rightarrow 29/2^+$
1878.7[d]	x		$37/2_1^+ \rightarrow 35/2^-$
2034.5	20(7)	0.92(38)	$41/2_2^- \rightarrow (37,39)/2^-$
2161.9	29(10)	0.80(34)	$41/2_2^- \rightarrow 39/2_1^-$
2233.0	122(14)	1.40(26)	$39/2_1^- \rightarrow 35/2^-$
2506.9	65(10)	1.60(40)	$37/2_1^+ \rightarrow 33/2_1^+$
2521.9	37(7)	0.28(16)	$(35,37)/2^+ \rightarrow 33/2_1^+$
2638.5	43(8)	1.21(40)	$37/2_3^+ \rightarrow 33/2_1^+$
2990.9	129(11)	0.58(14)	$37/2^- \rightarrow 35/2^-$
3454.8	17(7)	1.02(37)	$39/2_2^- \rightarrow 35/2^-$

[a]$\Delta E_\gamma = \pm(0.2-1.0)$ keV depending on the energy and intensity of the transition.
[b]The γ-ray intensity, I_γ, is corrected for detection efficiency and is normalized to 1000 for the 651.2 keV transition.
[c]The γ-ray anisotropy is defined as $R = 2I(143°)/[I(79°)+I(101°)]$.
[d]Not resolved.

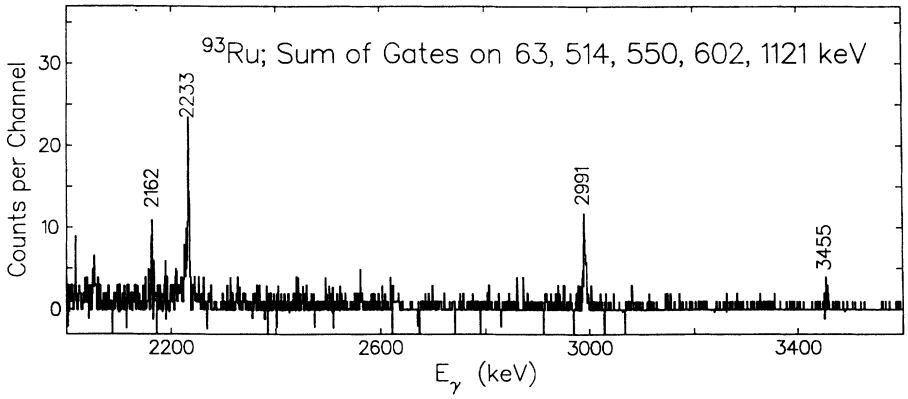

FIG. 10. Sum of ^{93}Ru $\gamma\gamma$-coincidence spectra gated by the 63, 514, 550, 602, and 1121 keV lines; the spectrum shows the high energy γ rays deexciting negative-parity levels above the energy gap at 6.0 MeV.

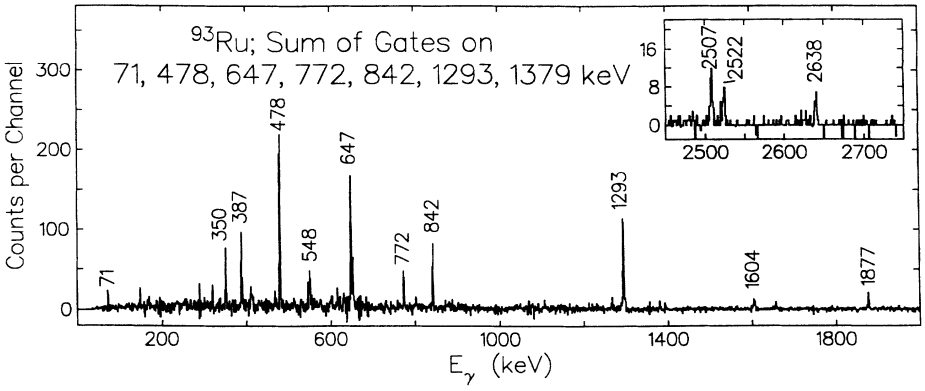

FIG. 11. Sum of ^{93}Ru $\gamma\gamma$-coincidence spectra with gates on the 71, 478, 647, 772, 842, 1293, and 1379 keV lines. The inset illustrates the high-energy γ rays deexciting the positive-parity levels above the energy gap at 5.4 MeV.

C. Results for ^{94}Rh

We presume that the ground state of ^{94}Rh has a spin value of 8^+ [8]. Our results as regards the decay scheme are shown in Fig. 12. Also here a characteristic feature of the yrast scheme is two decay sequences and the existence of energy gaps of the order of more than 2 MeV in each sequence. The $\gamma\gamma$ matrix obtained in the 187 MeV run was used in the analysis because of the better statistics in this experiment compared with the run at 147 MeV. The latter experiment, however, gave a cleaner matrix with much less "feedthrough" from channels of higher particle multiplicity due to their reduced cross sections at the lower beam energy. It can be expected that the negative-parity sequence enters the positive-parity sequence at the spin value 10^+ with an $E1$ transition (R value 0.7–0.8) from an 11^- state in analogy with the previous case of ^{92}Tc. As the 617 keV transition has the R value of a typical $E2$ transition, good candidates are the 563 and 696 keV transitions. The observation of a weak $E2$ crossover transition from the 13^- state to the 11^- state shows that the 696 keV transition represents the $E1$ transition.

The intensity differences of the transitions in the negative-parity sequence are not very helpful in establishing the order of the transitions; that given in Fig. 12 is the one preferred by the ESCL8R program. Energy gaps in both sequences are produced above the maximum spin values, 17, of the $p_{1/2},g_{9/2}$ configurations under the condition that the 44 keV transition in the positive-parity sequence is an $M1$ transition (in that case strongly converted). A coincidence spectrum gated by the 617 keV, $12^+\rightarrow 10^+$ transition shows a line with almost the same energy. We interpret this line as the $E2$ crossover transition $15^+\rightarrow 13^+$. A few $\gamma\gamma$ coincidence spectra are shown in Fig. 13. Table IV gives the γ-ray energies, relative intensities, and anisotropies. R values are plotted in Fig. 14.

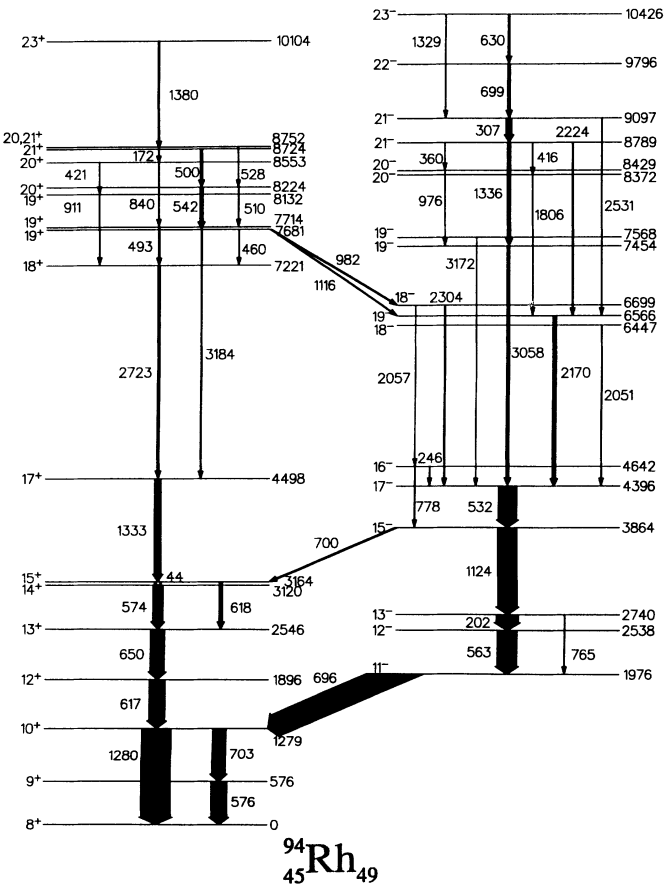

FIG. 12. Tentative level scheme for ^{94}Rh as produced in the ^{58}Ni(^{40}Ca,3pn)^{94}Rh reaction. Energies are in keV.

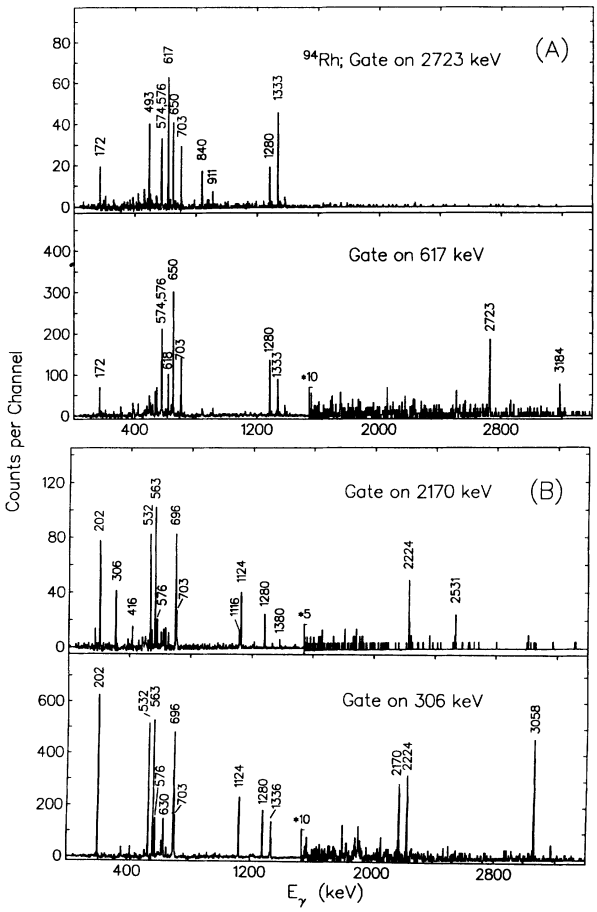

FIG. 13. Prompt $\gamma\gamma$-coincidence spectra of ^{94}Rh with (A) gates on the 2723 and 617 keV transitions showing the assumed positive-parity cascade and (B) gates on the 2170 and 306 keV transitions showing the assumed negative-parity cascade.

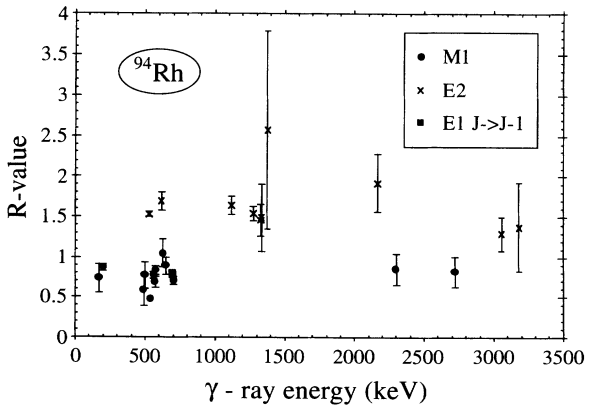

FIG. 14. γ-ray anisotropies, R (see text), plotted vs the energies of the γ-ray transitions in ^{94}Rh.

TABLE IV. Gamma-ray eneriges, intensities, and anisotropy ratios for γ-ray transitions assigned to ^{94}Rh.

E_γ[a] (keV)	I_γ[b]	R[c]	Tentative assignment $J_i^\pi \rightarrow J_f^\pi$	E_γ[a] (keV)	I_γ[b]	R[c]	Tentative assignment $J_i^\pi \rightarrow J_f^\pi$
44.2	41(12)		$15^+ \rightarrow 14^+$	699.9[d]			$15^- \rightarrow 15^+$
171.6	50(7)	0.73(18)	$21^+ \rightarrow 20_2^+$	703.2	513(23)	0.70(5)	$10^+ \rightarrow 9^+$
201.9	734(27)	0.87(4)	$13^- \rightarrow 12^-$	764.9	31(9)		$13^- \rightarrow 11^-$
246.0	60(10)	0.83(23)	$16^- \rightarrow 17^-$	777.9	36(10)		$16^- \rightarrow 15^-$
306.6	314(17)	0.82(7)	$21_2^- \rightarrow 21_1^-$	839.6	57(12)		$20_2^+ \rightarrow 19_2^+$
359.6	19(6)		$21_1^- \rightarrow 20_2^-$	910.9	37(10)		$19_3^+ \rightarrow 18^+$
416.4	22(7)		$21_1^- \rightarrow 20_1^-$	975.6	26(7)		$20_2^- \rightarrow 19_2^-$
420.6	25(7)		$20_2^+ \rightarrow 19_3^+$	982.3	65(20)		$19_1^+ \rightarrow 18_2^-$
460.2	28(8)		$19_1^+ \rightarrow 18^+$	1115.9	59(14)	1.64(32)	$19_1^+ \rightarrow 19_1^-$
492.5	96(15)	0.58(19)	$19_2^+ \rightarrow 18^+$	1124.1	889(40)	1.64(11)	$15^- \rightarrow 13^-$
500.2	120(13)	0.77(17)	$21^+ \rightarrow 20_1^+$	1279.8	1000(30)	1.54(9)	$10^+ \rightarrow 8^+$
510.1	40(14)		$20_1^+ \rightarrow 19_2^+$	1329.5	28(9)		$23^- \rightarrow 21_2^-$
528.4	20(7)		$20,21^+ \rightarrow 20_1^+$	1333.4	318(18)	1.46(20)	$17^+ \rightarrow 15^+$
531.7	882(33)	1.53(3)	$17^- \rightarrow 15^-$	1335.6	205(17)	1.49(41)	$21_1^- \rightarrow 19_2^-$
542.3	210(20)	0.47	$20_1^+ \rightarrow 19_1^+$	1379.7	101(24)	2.57(122)	$23^+ \rightarrow 21^+$
562.6	905(33)	0.77(4)	$12^- \rightarrow 11^-$	1806.1	20(9)		$20_1^- \rightarrow 19_1^-$
574.0	321(19)	0.68(7)	$14^+ \rightarrow 13^+$	2050.6	46(19)		$18_1^- \rightarrow 17^-$
576.4	497(23)	0.83(6)	$9^+ \rightarrow 8^+$	2056.5	17(9)		$18_2^- \rightarrow 16^-$
616.7[d]			$12^+ \rightarrow 10^+$	2170.2	203(20)	1.92(36)	$19_1^- \rightarrow 17^-$
	738(33)	1.69(11)		2223.5	52(20)		$21_1^- \rightarrow 19_1^-$
618.4[d]			$15^+ \rightarrow 13^+$	2303.6	73(10)	0.85(20)	$18_2^- \rightarrow 17^-$
630.3	168(17)	1.05(18)	$23^- \rightarrow 22^-$	2530.6	19(10)		$21_2^- \rightarrow 19_1^-$
650.2	529(38)	0.89(11)	$13^+ \rightarrow 12^+$	2723.4	122(15)	0.82(20)	$18^+ \rightarrow 17^+$
696.1	940(38)	0.79(5)	$11^- \rightarrow 10^+$	3057.7	187(17)	1.30(21)	$19_2^- \rightarrow 17^-$
698.3[d]			$22^- \rightarrow 21_2^-$	3172.1	15(7)		$19_3^- \rightarrow 17^-$
	219(22)	1.15(19)		3183.6	50(11)	1.38(55)	$19_1^+ \rightarrow 17^+$

[a]$\Delta E_\gamma = \pm(0.2-1.0)$ keV depending on the energy and intensity of the transition.
[b]The γ-ray intensity, I_γ, is corrected for detection efficiency and is normalized to 1000 for the 1279.8 keV transition.
[c]The γ-ray anisotropy is defined as $R = 2I(143°)/[I(79°)+I(101°)]$.
[d]Not resolved.

D. Results for ^{95}Pd

A 14 s, $\frac{21}{2}^+$ isomer was proposed by Nolte and Hick at an excitation energy of about 2 MeV [10]. The existence of this isomer was confirmed by Kurcewicz *et al.* [9] using the GSI on-line mass separator.

In our experiment a relatively clean $\gamma\gamma$ matrix could be obtained at 147 MeV although with limited statistics. For the spectroscopic work the $\gamma\gamma$ matrix obtained at 187 MeV was mainly used.

Of the few γ lines attributed to ^{95}Pd (see Table V) three γ lines have energies higher than 2.0 MeV (see Fig. 15), which supports the view that a long-lived isomeric state with an excitation energy of some MeV is populated and terminates the observed γ cascades. The expected yrast level spacing at low excitation energy, both in the positive- and negative-parity sequences, gives no space for high-energy γ-ray transitions, which are of the order of the gap energies observed for the earlier discussed nuclei. Using the calculated position of the $\frac{21}{2}^+$ state [3], the level scheme shown in Fig. 16 will result. In this scheme the 260 keV transition is proposed to be of electric dipole type. The complete decay chain [9,10] is schematically reproduced in Fig. 17.

TABLE V. Gamma-ray energies, intensities, and anisotropy ratios for γ-ray transitions assigned to ^{95}Pd.

E_γ[a] (keV)	I_γ[b]	R[c]	Tentative assignment $J_i^\pi \rightarrow J_f^\pi$
130.3	59(14)	0.64(10)	$25/2^+ \rightarrow 23/2^+$
260.4	39(14)	0.71(16)	$31/2^- \rightarrow 29/2^+$
382.0	8(2)		
465.1	13(3)		
556.0	11(2)		
680.0	46(15)	1.40(39)	$33/2^+ \rightarrow 29/2^+$
690.6	78(21)	1.12(20)	$23/2^+ \rightarrow 21/2^+$
821.3	9(3)		$25/2^+ \rightarrow 21/2^+$
1065	2(1)		
1374.3	100(15)	1.47(28)	$29/2^+ \rightarrow 25/2^+$
1517.9	29(12)		$(37-41)/2^+ \rightarrow (35,37)/2^+$
2087.9	35(13)		$(33,35)/2^- \rightarrow 31/2^-$
2110.9	41(14)		$(35-39)/2^- \rightarrow (33,35)/2^-$
2747.0	15(9)		$(35,37)/2^+ \rightarrow 33/2^+$

[a]$\Delta E_\gamma = \pm(0.2-1.0)$ keV depending on the energy and intensity of the transition.
[b]The γ-ray intensity, I_γ, is corrected for detection efficiency and is normalized to 100 for the 1374.3 keV transition.
[c]The γ-ray anisotropy is defined as $R = 2I(143°)/[I(79°)+I(101°)]$.

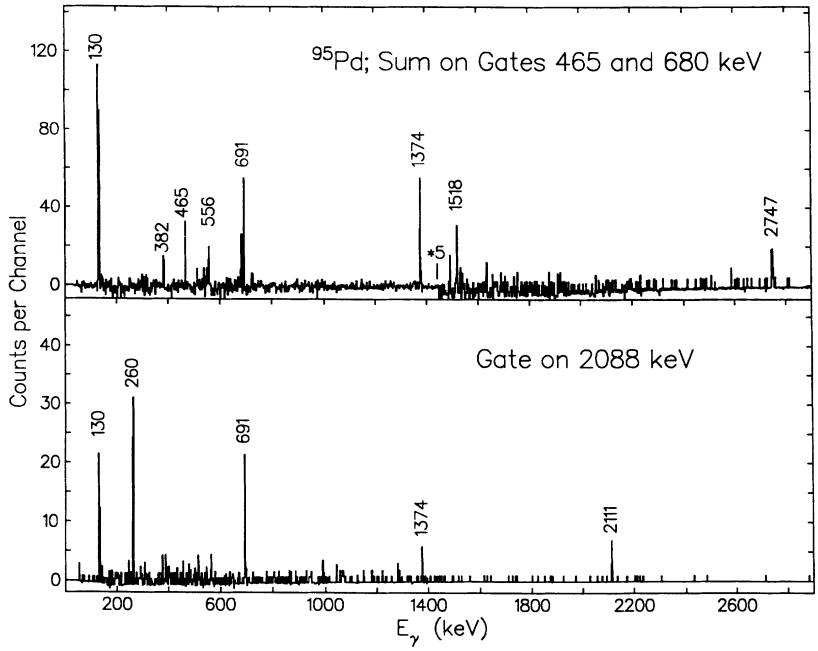

FIG. 15. Prompt $\gamma\gamma$-coincidence spectra of ^{95}Pd gated by the sum of the 465 and 680 keV transitions and by the 2088 keV transition, respectively.

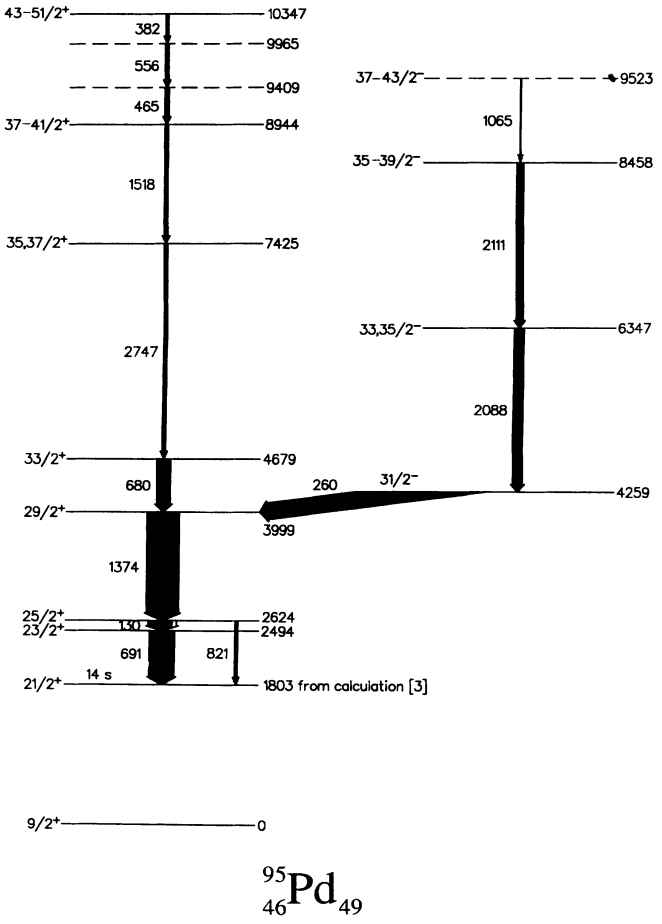

FIG. 16. Tentative level scheme for ^{95}Pd as produced in the ^{58}Ni(^{40}Ca,2pn)^{95}Pd reaction. Energies are in keV.

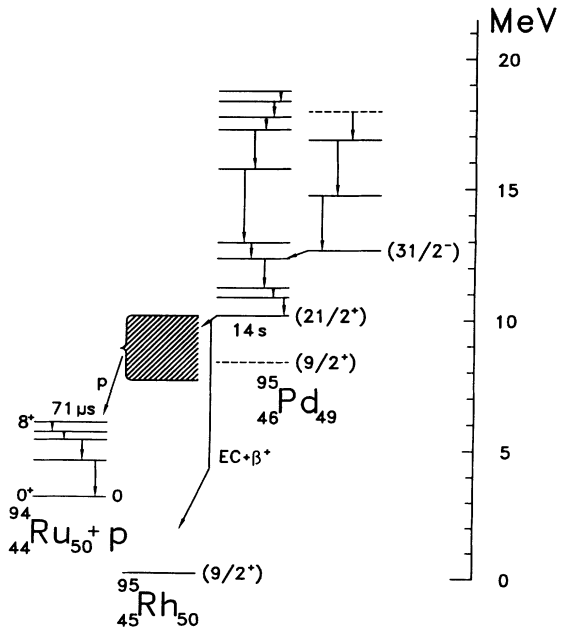

FIG. 17. The complete decay chain [9,10] of ^{95}Pd, shown schematically.

V. DISCUSSION

The use of multidetector arrays allows one to study the yrast level schemes of $Z,N \leq 50$ nuclei well up to and in favorable cases above the spin values attainable in the configuration space spanned by the $f_{5/2},p_{3/2},p_{1/2},g_{9/2}$ shells. It has thus become possible to compare experimental and theoretical yrast levels over an extended range of spin and excitation energy.

Some shell-model calculations have been performed for the $N=49$ nuclei. Serduke, Lawson, and Gloeckner [1], and Gross and Frenkel [2] calculated levels in ^{88}Y, ^{89}Zr, ^{90}Nb, ^{91}Mo, ^{92}Tc, and ^{93}Ru within the $p_{1/2},g_{9/2}$ configuration space. Recently, Sinatkas *et al.* [3] have made an extended shell-model calculation including all four orbitals $f_{5/2},p_{3/2},p_{1/2},g_{9/2}$ in the major shell between the magic numbers 28 and 50.

The experimental level schemes of the $N=49$ isotones ^{92}Tc, ^{93}Ru, ^{94}Rh, and ^{95}Pd, studied in the present work, all show distinct groups of low-energy levels of positive and negative parity, which are characterized by wave functions mainly belonging to the $\pi(p_{1/2},g_{9/2})^n \nu g_{9/2}^{-1}$ configurations with $n=5,6,7,8$, respectively. These groups are separated by energy gaps from the higher-spin levels, which are believed to be formed by either exciting one proton from the deeper $f_{5/2},p_{3/2}$ shells across the $Z=38$ gap into the $p_{1/2},g_{9/2}$ shells or by exciting one neutron from the $g_{9/2}$ shell across the $N=50$ gap up to the $d_{5/2}$ shell. We have calculated the maximum-spin neutron-excited states of both parities, and find good agreement with the experimental energies of the highest observed levels in ^{93}Ru, ^{94}Rh, and ^{95}Pd.

We now proceed to a discussion of the level structure in each $N=49$ nucleus separately.

A. Discussion of levels in ^{92}Tc

The experimental energies are compared with the calculated energies of Sinatkas *et al.* [3] in Fig. 18. The agreement is good for the positive-parity levels with $J \leq 15$, which are all dominated by the $\pi(p_{1/2}^2 g_{9/2}^3)\nu g_{9/2}^{-1}$ configuration. The level at 5645 keV corresponds to the configuration $\pi g_{9/2}^5 \nu g_{9/2}^{-1}$ with the protons coupled to the seniority -5, $\frac{25}{2}^+$ state and the total spin is 16 or 17. The energies of the negative-parity levels up to 17^- with the principal configuration $\pi(p_{1/2}g_{9/2}^4)\nu g_{9/2}^{-1}$ also agree within about ± 100 keV.

The two observed levels above 6 MeV both probably belong to the configuration group $\pi(f_{5/2},p_{3/2})^{-1}\pi(p_{1/2},g_{9/2})^6 \nu g_{9/2}^{-1}$. The calculated yrast 18^+ and 19^+ states can be described as the 1836 keV 2^+ excitation of the ^{88}Sr core, coupled to the 16^+ and 17^+ states of the $\pi g_{9/2}^5 \nu g_{9/2}^{-1}$ configuration. Similar states with the 2^+ core excitation built on an empty $\pi p_{1/2}$ shell, and combined with a $\pi g_{9/2}^n$ configuration, are known in the lighter $N=50$ nuclei ^{89}Y ($\frac{11}{2}^+$ and $\frac{13}{2}^+$) and ^{90}Zr (9^+ and 10^+), and the $N=49$ nuclei ^{88}Y (10^+ and 11^+) and ^{89}Zr ($\frac{25}{2}^+$ and $\frac{27}{2}^+$). Based on the empirical values of the interaction energy between the 2^+ excitation and the single particle $\pi g_{9/2}$ and the single hole $\nu g_{9/2}^{-1}$, derived from these data, one can estimate that the 18^+ and 19^+ states in ^{92}Tc should both come about 1800 keV above the 17^+ state. The experimental level at 7431 keV can be identified with either one of these two states.

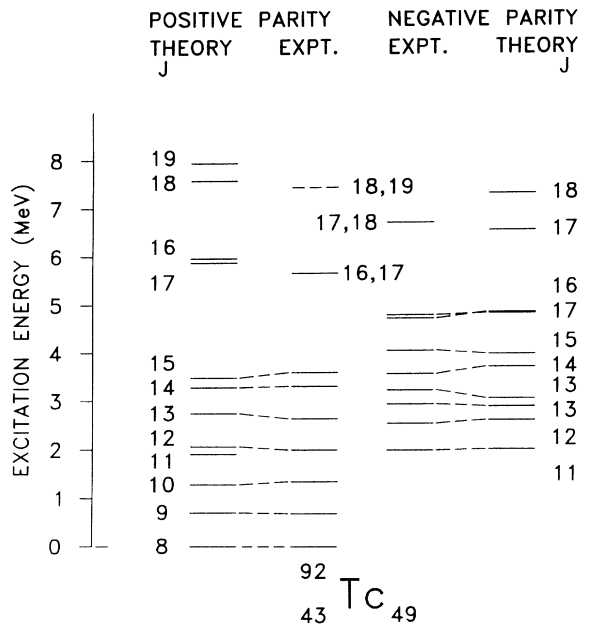

FIG. 18. Comparison between calculated [3] and experimentally established yrast levels in ^{92}Tc. Dashed lines connect theoretical and experimental yrast levels of the same spin and parity.

The negative-parity level at 6702 keV can be understood as a proton hole $\pi f_{5/2}^{-1}$ or $\pi p_{3/2}^{-1}$ combined with the configuration $\pi(p_{1/2}^2 g_{9/2}^4)\nu g_{9/2}^{-1}$. The fact that the decay goes mainly to the 16^- level and not to the nearby 17^- level indicates that the $\pi(p_{1/2}^2 g_{9/2}^4)\nu g_{9/2}^{-1}$ structure is coupled to $\frac{31}{2}^+$. The 1986 keV transition corresponds either to the $\pi f_{5/2}^{-1} \rightarrow \pi p_{1/2}^{-1}$ $E2$ transition if the total spin of the initial state is 18, or to the $\pi p_{3/2}^{-1} \rightarrow \pi p_{1/2}^{-1}$ $M1$ transition if the total spin is 17.

B. Discussion of levels in ^{93}Ru

The levels of positive and negative parity below 7 MeV excitation energy are all understood as belonging to the configurations $\pi(p_{1/2},g_{9/2})^6 \nu g_{9/2}^{-1}$. The calculated energies of Sinatkas *et al.* [3] are compared with the experimental data in Fig. 19. The positive-parity levels up to and including the yrast $\frac{33}{2}^+$ level at 5342 keV have all the principal configuration $\pi(p_{1/2}^2 g_{9/2}^4)\nu g_{9/2}^{-1}$. The energy agreement is within about ± 100 keV for all thirteen levels.

The second $\frac{33}{2}^+$ level at 6377 keV can only be interpreted as the $\pi g_{9/2}^6 \nu g_{9/2}^{-1}$ state with maximum spin. The calculated energy for this state is about 400 keV too high compared to the $\pi(p_{1/2}^2 g_{9/2}^4)\nu g_{9/2}^{-1}$ states. We note that the empirical matrix elements derived in [1,2] give a much better relative energy for this state.

The negative-parity levels below 7 MeV are well described as mainly $\pi(p_{1/2}g_{9/2}^5)\nu g_{9/2}^{-1}$ states. The calculated energies in Fig. 19 are all systematically about 200 keV too high, compared to those of positive parity.

A complex spectrum has been observed above 7 MeV. Most of these levels are classified as neutron core excita-

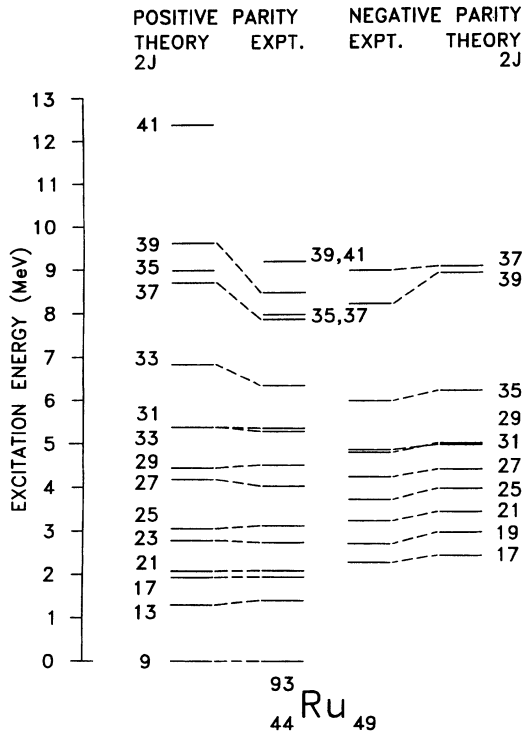

FIG. 19. Comparison between theoretically predicted [3] and the experimentally established yrast levels in ^{93}Ru. Dashed lines connect theoretical and experimental yrast levels of the same spin and parity.

tions $\nu d_{5/2}g_{9/2}^{-1}$ combined with the lower-lying $\pi(p_{1/2},g_{9/2})^6\nu g_{9/2}^{-1}$ states. However, three of the levels, at 7981, 8204, and 8331 keV, are considered to belong to the $\pi(f_{5/2},p_{3/2})^{-1}\pi(p_{1/2},g_{9/2})^7\nu g_{9/2}^{-1}$ category. The $\frac{37}{2}^+$ level at 7981 keV is characterized as the 2^+ excitation of the ^{88}Sr core, coupled to the $\frac{33}{2}^+$ (6377 keV) state with an empty $\pi p_{1/2}$ shell. This interpretation is supported both by the agreement of the excitation energy calculated with the empirical interactions, and by the preferred decay to the $\frac{33}{2}^+$ (6377 keV) state, which has a $B(E2)$ value 20 times larger than the transition to the lower $\frac{33}{2}^+$ (5342 keV) state.

The negative-parity levels at 8204 and 8331 keV are interpreted as states with a proton hole $\pi f_{5/2}^{-1}$ or $\pi p_{3/2}^{-1}$ coupled to the configuration $\pi(p_{1/2}^2 g_{9/2}^5)\nu g_{9/2}^{-1}$. Since there is only one $\frac{39}{2}^-$ state of this kind, and since we prefer to identify it with the 8204 keV level, the 8331 keV level is best assigned $\frac{37}{2}^-$. The R values have too large errors to decide which is the correct assignment.

Most of the higher levels are assumed to belong to the configuration group $\pi(p_{1/2},g_{9/2})^6\nu(d_{5/2}g_{9/2}^{-2})$. No detailed calculation of these levels is available. We have, however, calculated the energies of the highest-spin states in this group, $\frac{45}{2}^+$ and $\frac{47}{2}^-$, each with a simple, unique coupling scheme. The primary neutron core excitations $\nu d_{5/2}g_{9/2}^{-1}$ have been identified in ^{88}Sr and ^{90}Zr by neutron transfer reactions [17]. Using this information, combined with empirical matrix elements for the interaction of the neutron particle $\nu d_{5/2}$ and the neutron hole $\nu g_{9/2}^{-1}$ with the protons in the $\pi p_{1/2}$ and $\pi g_{9/2}$ shells, we calculated the energies $E(\frac{45}{2}^+)=10\,860$ keV and $E(\frac{47}{2}^-)=11\,960$ keV. The excellent agreement of these values with the experimental energies for the highest observed states of the positive and negative parity gives us confidence that these levels are correctly identified. The top levels decay by cascades of allowed $M1$ and $E2$ transitions to lower states within the same configurations, until other transitions proceeding by configurational impurities become more favorable.

C. Discussion of levels in ^{94}Rh

All levels of positive and negative parity below 5 MeV are characterized as members of the $\pi(p_{1/2},g_{9/2})^7\nu g_{9/2}^{-1}$ configuration group. Since Sinatkas *et al.* [3] did not calculate states in this nucleus, we have ourselves calculated the energies of the highest few states, using the matrix elements of Serduke *et al.* [1]. The results are

$$E(17^+)=4443 \text{ keV},$$

$$E(17^-)=4458 \text{ keV},$$

$$E(16^-)=4695 \text{ keV}.$$

A full shell-model calculation for the lower states would be useful to check if the energy agreement is of a similar quality as in ^{92}Tc and ^{93}Ru.

Among the higher levels we suggest that the three negative-parity levels at 6447, 6566, and 6699 keV have a proton hole of $\pi f_{5/2}^{-1}$ or $\pi p_{3/2}^{-1}$ coupled to the configuration $\pi(p_{1/2}^2 g_{9/2}^6)\nu g_{9/2}^{-1}$. The maximum spin for this type of state with a proton hole $\pi f_{5/2}^{-1}$ is 19, and the level at 6566 keV is identified as this state. The 2170 keV $E2$ transition $19^-\rightarrow 17^-$ in ^{94}Rh then corresponds to the 2233 keV $E2$ transition $\frac{39}{2}^-\rightarrow\frac{35}{2}^-$ in ^{93}Ru. The 18^- level at 6699 keV is naturally identified with the $\pi f_{5/2}^{-1}$ type state with one unit less than maximum spin, since it lies above the 19^- level and decays to both 16^- and 17^-. The 18^- level at 6447 keV must be the $\pi p_{3/2}^{-1}$ type state with maximum spin, decaying by a fast $M1$ transition $\pi p_{3/2}^{-1}\rightarrow\pi p_{1/2}^{-1}$ to 17^-.

Most of the higher levels above 7 MeV are assumed to belong to the configuration group $\pi(p_{1/2},g_{9/2})^7\nu(d_{5/2}g_{9/2}^{-2})$. Using the same input data as in the case of ^{93}Ru we have calculated the energies of the highest-spin states in the group. The results, $E(23^+)=10\,050$ keV and $E(23^-)=10\,450$ keV, are also here in excellent agreement with the experimental energies for the highest observed levels of positive and negative parity. This supports our belief that the states have been correctly identified, and connects the top of the observed yrast structures of ^{93}Ru and ^{94}Rh.

D. Discussion of levels in ^{95}Pd

The observed levels below 5 MeV are all definitely members of the $\pi(p_{1/2},g_{9/2})^8\nu g_{9/2}^{-1}$ configuration group. The calculated excitation energies of Sinatkas *et al.* [3] are compared with the experimental data in Fig. 20. The

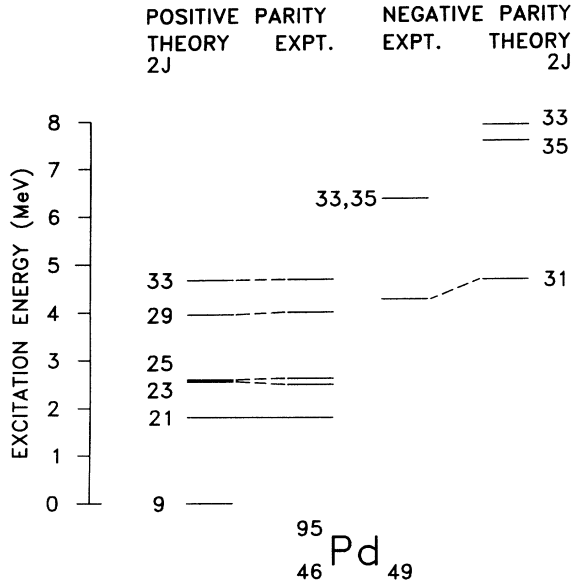

FIG. 20. Experimental yrast levels and yrast levels predicted by Sinatkas *et al.* [3] for ^{95}Pd. Dashed lines connect theoretical and experimental yrast levels of the same spin and parity. Note that the experimental value of the $\frac{21}{2}_1^+$ state is not known. In the figure the value 1803 keV calculated by Sinitkas *et al.* [3] for the energy of this state has been used. All other level positions in the figure are thus given in relation to the value 1803 keV.

agreement is very good for the five observed positive-parity levels, from the $\frac{21}{2}^+$ β-decaying isomer up to the $\frac{33}{2}^+$ maximum-spin state. The $\frac{31}{2}^-$ negative-parity state with maximum spin is calculated about 400 keV too high, a deviation in the same direction as noted for ^{93}Ru.

The level at 6347 keV is interpreted as the $\frac{35}{2}^-$ maximum-spin state of the $\pi(f_{5/2}^{-1}p_{1/2}^2 g_{9/2}^7)\nu g_{9/2}^{-1}$ configuration. The $\frac{35}{2}^- \rightarrow \frac{31}{2}^-$ transition energy, 2088 keV, falls nicely into the systematics of the equivalent $E2$ transitions in ^{93}Ru and ^{94}Rh.

For intensity reasons it has not been possible to establish the higher part of the level scheme of ^{95}Pd with the same detail as in ^{93}Ru and ^{94}Rh. However, there is a clear cascade of coincident gammas on the positive-parity side, which defines a highest level at 10 347 keV. By similar methods as used for ^{93}Ru and ^{94}Rh we have calculated the energy of the state $\pi(p_{1/2}^2 g_{9/2}^6)\nu(d_{5/2}g_{9/2}^{-2})$ with maximum spin. The result, $E(\frac{45}{2}^+)=10\,300$ keV, allows us to identify this state with the highest observed level. On the negative-parity side the calculated energy of the state $\pi(p_{1/2}g_{9/2}^7)\nu(d_{5/2}g_{9/2}^{-2})$ with maximum spin is $E(\frac{43}{2}^-)=10\,400$ keV. Apparently this level has not been excited with sufficient intensity to be observed in this experiment.

VI. SUMMARY

We have studied the $N=49$ isotones ^{92}Tc, ^{93}Ru, ^{94}Rh, and ^{95}Pd produced in ^{40}Ca+^{58}Ni fusion reactions. The multidetector system NORDBALL at NBI, Risø, was used with 15 BGO-shielded HPGe γ detectors, a charge particle identification system comprising 21 Si detectors, and 11 liquid scintillator neutron detectors.

We have extended the level scheme in ^{92}Tc from 12^+ to $\geq 18^+$ and $\geq 17^-$, and in ^{93}Ru from $\frac{21}{2}^+$ and $\frac{17}{2}^-$ to $\geq \frac{45}{2}^+$ and $\frac{47}{2}^-$. For ^{94}Rh, where previously only an 8^+ and a 3^+ level (g.s. and isomer) were known, we have identified states up to 23^+ and 23^-. In ^{95}Pd, where only the $(\frac{21}{2}^+)$ β-decaying isomer has been seen, we found levels up to $\geq \frac{43}{2}^+$ and $\geq \frac{37}{2}^-$.

We have compared our level schemes with the shell-model calculations of Sinatkas *et al.* except for ^{94}Rh, for which their results were not available. For the levels of moderate spin, the restricted shell-model space spanned by the $\pi(p_{1/2})$, $\pi(g_{9/2})$, and $\nu(g_{9/2})^{-1}$ orbitals gives a very good (better than 100 keV) agreement with our results for positive-parity levels, whereas the theoretical energies for negative-parity levels tend to be somewhat too high.

The main new results of our work concern higher levels with spin outside this restricted shell-model space (cf. Table I). There are two straightforward possibilities to enlarge the space, either by promoting one proton from the $p_{3/2}$ or $f_{5/2}$ to the $p_{1/2}$ orbit, or—more radically—to excite one neutron across the $N=50$ shell closure to form a $\nu(g_{9/2}^{-2}d_{5/2})$ configuration. Whereas the former procedure only adds 1 or 2 units of spin, the latter adds up to 6 units when fully aligned with the proton configuration. Some indication of the energy needed for a neutron particle-hole excitation is given by the energy of the 7^+ state of ^{88}Sr, 5.10 MeV.

It is a striking common feature of our level schemes that they show a gap of about 2 MeV at 6–7 MeV excitation energy, just above the level that represents the maximum spin in the restricted configuration space. Also, the maximum spin we observe in three cases (^{93}Ru, negative parity, and ^{94}Rh, both parities) is equal to the maximum obtainable with the neutron particle-hole included. In three other cases, our possible experimental spin range covers the maximum, viz. ^{93}Ru, positive parity, and ^{95}Pd, both parities. Furthermore, the energy difference between the fully aligned configurations of the two spaces is rather constant, 5.60±0.07 MeV for the positive parities, and 6.00±0.03 MeV for the negative parities.

In all four nuclei there is evidence for excitation of the $\pi p_{3/2}$ and/or the $\pi f_{5/2}$ orbital. These states decay by $M1$ or $E2$ transitions of about 2 MeV to the highest observed levels of the restricted space.

A result of this experimental investigation is that a number of new levels can be accurately described as $\pi(p_{1/2},g_{9/2})^n\nu g_{9/2}^{-1}$ states in analogy with the previously established situation for the $\pi(p_{1/2},g_{9/2})^n$ states in the $N=50$ isotones. Also, at higher spin and energy, we have observed a number of levels which can be qualitatively understood as states formed by exciting, in addition, either a proton from the $p_{3/2}$ or $f_{5/2}$ shell or a neutron into the $d_{5/2}$ shell.

ACKNOWLEDGMENTS

The authors are grateful to the staff of the Niels Bohr Institute, Risø, for their hospitality and for providing

beams and technical support. We are especially indebted to Jörn Westergaard for operating the NBI Tandem van de Graaff and booster accelerator system. We are very thankful to Dr. L. D. Skouras, Athens, for sending us the results of the shell-model calculations prior to publication. We also want to thank Dr. D. C. Radford for giving us access to his very useful computer program ESCL8R. The support from the Swedish Natural Science Research Council (NFR), the Danish Natural Science Research Council (SNF), and the Japanese government is greatly appreciated.

[1] F. J. D. Serduke, R. D. Lawson, and D. H. Gloeckner, Nucl. Phys. **A256**, 45 (1976).
[2] R. Gross and A. Frenkel, Nucl. Phys. **A267**, 85 (1976).
[3] J. Sinatkas, L. D. Skouras, D. Strottman, and J. D. Vergados, J. Phys. G **18**, 1401 (1992).
[4] S. E. Arnell, T. Kuroyanagi, S. Mitarai, J. Nyberg, H. A. Roth, and Ö. Skeppstedt, in *Nuclear Physics in the Nineties,* Oak Ridge, Tennessee, Proceedings, Vol. 1, p. 214 (1990).
[5] C. A. Fields, F. W. N. de Boer, and B. J. Diana, Nucl. Phys. **A401**, 117 (1983).
[6] A. Nilsson and M. Grecescu, Nucl. Phys. **A212**, 448 (1973).
[7] H. Sievers, Nucl. Data Sheets **54**, 99 (1988).
[8] K. Oxorn, B. Singh, and S. K. Mark, Z. Phys. A **294**, 389 (1980).
[9] W. Kurcewicz, E. F. Zganjar, R. Kirchner, O. Klepper, E. Roeckl, P. Komninos, E. Nolte, D. Schardt, and P. Tidemand-Petersson, Z. Phys. A **308**, 21 (1982).
[10] E. Nolte and H. Hick, Z. Phys. A **305**, 289 (1982).
[11] F. Pühlhofer, Nucl. Phys. **A280**, 267 (1977).
[12] B. Herskind, Nucl. Phys. **A447**, 395c (1985).
[13] T. Kuroyanagi, S. Mitarai, S. Suematsu, B. J. Min, H. Tomura, J. Mukai, T. T. Maeda, R. Nakatani, G. Sletten, J. Nyberg, and D. Jerrestam, Nucl. Instrum. Methods **A316**, 289 (1992).
[14] S. E. Arnell, H. A. Roth, Ö Skeppstedt, J. Bialkowski, M. Moszynski, D. Wolski, and J. Nyberg, Nucl. Instrum. Methods **A300**, 301 (1991).
[15] D. C. Radford, private communication; D. C. Radford *et al.*, Nucl. Phys. **A545**, 665 (1992).
[16] A. E. Blaugrund, Nucl. Phys. **88**, 501 (1966).
[17] P. C. Li and W. W. Daehnick, Nucl. Phys. **A462**, 26 (1987).